Title of paper:

The influence of grass roots on the shear strength of pyroclastic soils

Author's affiliation and address:

Name: Vito Foresta

Affiliation: Department of Civil and Engineering, University of Salerno

Address: via Giovanni Paolo II 132, 84084 Fisciano (SA), Italy

E-mail: vforesta@unisa.it

Name: Vittoria Capobianco

Affiliation: Norwegian Geotechnical Insitute

Address: P.O. Box 3930 Ullevål Stadion, NO-0806 Sognsveien 72, Oslo, Norway

E-mail: vittoria.capobianco@ngi.no

Name: Leonardo Cascini

Affiliation: Department of Civil and Engineering, University of Salerno

Address: via Giovanni Paolo II 132, 84084 Fisciano (SA), Italy

E-mail: l.cascini@unisa.it

Author responsible for correspondence:

Name: Vittoria Capobianco

Address: P.O. Box 3930 Ullevål Stadion, NO-0806 Sognsveien 72, Oslo, Norway

Telephone number: +39 3200867247

E-mail: vittoria.capobianco@ngi.no

The influence of grass roots on the shear strength of pyroclastic soils

Abstract: The paper investigates the effects of indigenous vegetation on the shear strength of loose pyroclastic soils of the Campania region (Southern Italy); these soils are frequently affected by shallow landslides 1-2m deep that experience static liquefaction during the post-failure stage. Perennial *graminae* grasses were seeded in a 1D column 2 m high and filled by pyroclastic soils, allowing the root to grow under atmospheric conditions. A noninvasive sampling procedure was adopted to take the vegetated soil samples, in which the roots were in their natural geometrical distribution. For each rooted sample, the root biomass *RM* was measured, and the root volume density *RVD* was calculated. Isotropic consolidated triaxial tests in both drained and undrained conditions were performed on the rooted specimens, as well as on bare specimens as a control. The obtained results showed that the roots generally provided an increment to the soil strength. In drained conditions a reduction in the volumetric deformation was observed, which, under undrained conditions, was reflected in a general reduction of the excess pore water pressures with a possible inhibition of the static liquefaction occurrence. This study highlights the potential role of grass roots as bio-engineering practice for stabilizing shallow covers of pyroclastic soils.

Key words: failure, vegetation, triaxial tests, shallow landslides, liquefaction.

INTRODUCTION

Shallow flow-type landslides (Hungr et al. 2001) are widely recognized as catastrophic events. They generally occur on natural hillslopes covered by residual (Lim et al. 1996; Toll et al. 1999), colluvial (Campbell 1975), weathered (Meisina 2006) or pyroclastic deposits (Capra et al. 2003;

Cascini et al. 2008; Cascini et al. 2013). The first failure stage is often caused by rainfall infiltration (De Vita and Reichenbach 1998; Matsushi et al. 2006) in combination with other factors, such as the geology and the morphology of the slopes, as well as the hydrological properties of the shallowest soil layers (Reid et al. 1988). The post-failure stage can be characterized by a rapid mass movement, which behaves such as a fluid that can cover great distances, threating human lives, activities and infrastructures (Silde and Ochiai 2006; Keefer and Larsen 2007).

In pyroclastic soils originating from the Somma-Vesuvius eruptions in the Campania region (South Italy), during the post-failure stage of shallow landslides a volume collapse of the soil structure can occur in fully saturated undrained conditions. This collapse causes a significant increment in the pore-water pressures that cannot freely dissipate, leading to the annulment of the mean effective stresses and, thus, to the soil's static liquefaction (Wang et al. 2002; van Asch et al. 2006; Olivares and Damiano 2007). Therefore, the unstable mass evolves into a flow during the propagation stage (Cascini et al. 2010).

Structural passive control works, such as dissipative basins and/or brindles, have been widely adopted as risk mitigation measures for these flow-like landslides (Versace 2008), even if they are expensive and require frequent maintenance. The use of indigenous vegetation can represent a sustainable bio-engineering alternative for stabilizing shallow pyroclastic covers because of the well-known role of roots in enhancing the shear strength of soil.

Vegetation enhances soil stability through both hydrological and mechanical reinforcement. The roots, indeed, promote the soil water extraction via the transpiration process, thus preserving the unsaturated conditions that reduce the probability of occurrence of the first failure stage. This positive hydrological effect has been recently proven by experimental and numerical studies on

the variation of hydraulic properties of root permeated soils (Ng et al. 2018; Ng et al. 2016; Ni et al. 2018).

Many authors in the past investigated the mechanical reinforcement of roots on slope stability through both in situ and laboratory direct shear tests (Endo and Tsuruta 1969; Ziemer 1981; Nilaweera 1994; Wu et al. 1988; Tobias 1995; Wu and Watson 1998; Operstein and Frydman 2000; Comino et al. 2010; Yildiz et al. 2018), providing substantial insights into the reinforcement role of roots in the drained shear strength of soils. This reinforcement is widely considered as an additional soil strength via root cohesion (Wu et al. 1979; Nilaweera and Nutalaya 1999; Cazzuffi et al. 2006; Wu 2013; Leung et al. 2015), rather than the internal friction angle variation, which seems slightly affected by roots (Waldron 1977). Despite the fact that the direct shear test is often adopted for the assessment of the shear strength of root-reinforced soils, the limitation of using this method is given by *i)* the assumed failure plane and *ii)* the undrained conditions not being reproduced. Conversely, in triaxial tests the failure surface is generated along the weakest surface and different drainage conditions (i.e., drained, undrained) can be simulated to closely reproduce the in situ conditions (Zhang et al. 2010).

Few triaxial tests have been conducted on root-soil composite samples in recent years (Frei 2009; Graf et al. 2009; Zhang et al. 2010; Liu et al. 2011; Hu et al. 2013), which confirmed the positive role of roots on increasing the shear strength of the reinforced soil. Nevertheless, some controversial results are available depending on the soil type, vegetation type and its orientation in the soil mass (Graf et al. 2009; Zhang et al. 2010; Hu et al. 2013). In fact, triaxial tests involve some issues related to the preparation of root-soil composite specimens, such as the geometry, the length and/or the root's orientation (i.e., horizontal, crossed, vertical), which sometimes do not well reproduce the natural root distribution (Zhang et al. 2010; Hu et al. 2013), thus affecting the

experimental results. Moreover, for grass roots the effects on the soil shear strength as well as on the soil structure modification are still not clear, since it is difficult to artificially reproduce their distribution in soil specimens. Some studies have found that grass roots can change the entire soil matrix by creating a dense but extremely light root network that indirectly increments soil aggregates via exudates and the production of microbial communities (Jastrow et al. 1998; Eisenhauer et al. 2010).

Few contributions are available on the behavior of loose rooted soils under undrained conditions, and the effects of the root presence on the occurrence of static liquefaction in undrained conditions has yet to be investigated. To this aim, an experimental program based on triaxial tests on rooted pyroclastic soils was set up, considering both drained and undrained conditions that closely reproduce the failure conditions in shallow pyroclastic covers. Isotropic consolidated drained triaxial tests in saturated conditions simulate the typical failure of rainfall-induced landslides, while undrained triaxial tests allow us to investigate the influence of roots during the post-failure stage, when static liquefaction can occur.

MATERIALS AND METHODS

Experimental set-up, soil type and preparation

The equipment consisted of a hollow Plexiglas column with an inner and outer diameter of 192 mm and 200 mm, respectively, with a total height of 2 000 mm (Fig. 1). The side boundaries were impermeable and the top boundary was exposed to the atmosphere. Free drainage was allowed through a series of 3 mm diameter holes at the bottom of the column, where a geosynthetic layer was placed to avoid the possible exit of fine grains during the water flow. The column was divided into 4 equal blocks, each 500 mm in height and linked to one another by flanged bases for

facilitating both the initial filling and the final sampling procedures. The blocks were called A, B, C, and D, starting from the bottom of the column. The column was filled to a depth of 1 900 mm, while the top 100 mm were left empty for protection of the foliage and for water applications during plant growth (Fig. 1).

The pyroclastic soil analyzed in this study was originated from the past explosive phases of the Somma-Vesuvius volcano (Lirer et al. 2001; Cioni et al. 1999), which covers the limestones and volcanic rock slopes over an area of approximately 3,000 square kilometers of the Campania region (Southern Italy). The soil was collected from the pyroclastic deposits covering the Pizzo D'Alvano massif in the source area of the Tuostolo debris flow (Fig. 2). This landslide was one of the several debris flows that occurred during the May 1998 event, which caused a loss of lives as well as huge damages to the towns located at its piedmont (Cascini et al. 2011).

Such deposits have been classified by Bilotta et al. (2005) in two main classes, depending on their grain size, physical and mechanical properties. According to the graphical settings of most of the pyroclastic mantles on volcanic rock slopes (Revellino et al. 2004; Bilotta et al. 2005; Cascini et al. 2008; Ferlisi et al. 2016), coarser volcanic ashy soils generally belong to the superficial layers (2 – 3 m) and overlay the finest class of deposits, with some presence of interbedded pumice layers. The soil collected and investigated in this study belongs to the volcanic ashy soils typical of superficial layers, with gravel, sand, silt and clay contents of 8.1%, 60.2%, 30.6% and 1.1%, respectively. It can be classified as sand with silt according to the Unified Soil Classification System USCS (ASTM, 2010). The material is non-plastic soil with a specific gravity (G_s) equal to 2.59, which is included in the typical range of specific gravity values for the coarser ashy materials from 2.45 to 2.70, and with a liquid limit equal to 40.6% (Bilotta et al. 2005). To reduce the disturbance of the sampling of specimens for triaxial tests (BS 1377-8 1990), only soil with particle

size $d < 9.525$ mm was used to fill the column, thus filtering the particles that were present in the soil with a percentage lower than 1%.

The moist tamping method (Ladd 1977) was adopted to compact the soil in the column by fixing a target bulk density of 12.03 kN/m^3, and a gravimetric water content of 10%. The related porosity n was 53.5%, for which the investigated soil can experience collapse in unsaturated conditions under wetting (Nicotera et al.1998; Bilotta et al. 2006; 2008; Lancellotta et al. 2012).

Vegetation species

The selected vegetation type belongs to the perennial *graminae* grasses, which are indigenous and commonly involved in bio-engineering practices for soil surface protection, as well as in ecological restoration. This bushy perennial *graminae* can have a radial gravitropic vegetative growth in vertical direction (Bonneu et al. 2012) and a fascicle (alias fibrous) root system generally rooting downward from the plant body, capable of reaching great depths. The *graminae* was seeded in a small pot, germinated for 1 month in a greenhouse with a daily water supply, and then transplanted to the column. The transplanting period was at the end of January 2016 and the initial mean root depth was 6.0 ±0.3 cm, while the average height of the foliage was 8.0 ±0.2 cm.

A total of 3.5 g of seeds were also spread on the soil surface of the column in order to increase the number of *graminae* grasses that could grow within the soil column. Finally, the first irrigation was completed. The column was placed under atmospheric conditions outside the Geotechnical Laboratory "Giuseppe Sorbino" of the University of Salerno (40°46'14.5'' N, 14°47'21.4 E), under a rainout shelter to protect it from direct rainfall. The irrigation was made by an automatic irrigation system (T 1030 D, Gardena Water Timer electronic), which was properly programmed to provide the amount of 1 liter of water every second day, while from June to September twice a

day. During the first vegetative year, the average root depth and height of the foliage were visually monitored every month using a graduated scale placed along the transparent surface of the column. By the end of the summer (September 2016), the roots had already reached the bottom of the column (block A in Fig. 1).

Preparation of the samples

After one vegetative year, the sampling of the rooted soils began. The samples were obtained starting from the bottom after having placed the entire soil column along a horizontal plane. Then, the soil at the interface between the first two adjacent blocks (A, B) was cut with a plain steel string 0.28 mm in diameter and the block A was brought inside the Laboratory, while the remaining part of the column (only consisting in blocks B,C,D) was again placed outdoor to keep the vegetation alive until the next block (B) to be cut and so forth (C and D).

For the sampling of the triaxial specimens, the isolated block was positioned vertically and the soil was moved, with the help of a piston, into Plexiglas cylinders with the same inner diameter of the column and a height of either 100 mm or 200 mm. Since each block was 500 mm high, two 200 mm and one 100 mm cylinders were needed.

The aim of dividing a 500 mm high block in two 200 mm high and one 100 mm high cylinders was *i)* to have different sampling depths for each block, *ii)* to minimize the disturbance due to possible loosening of soil due to roots breakage during the sampling of triaxial specimens and *iii)* to have a cylinder as the control of the representativeness of the rooted soil specimens used in triaxial tests.

Among the two 200 mm high cylinders obtained for each block, one cylinder was utilized for triaxial tests, whereas the remaining cylinders were covered at both the upper and lower boundaries

and opportunely sealed to maintain the initial soil water content and to preserve roots from imminently decaying.

In total, four 200 mm high cylinders, one for each block, were used for the triaxial tests. The undisturbed root-soil samples were taken through a rigid plastic sampler 36.4 mm in diameter and 210 mm in length. The sampler was intruded into the rooted soil with a low penetration velocity to gently cut the lateral roots and prevent the soil from being dragged by the lateral roots that had not yet broken. From each sampler, 2 undisturbed soil specimens 79.3 mm in height and 36.4 mm in diameter were obtained. In total, 19 undisturbed root-soil specimens were used for the triaxial tests. Moreover, six bare soil specimens were reconstituted through a moist tamping technique with the same target bulk density used for filling the soil column. These bare specimens were used as the control to quantify the effect of roots on the soil shear strength.

Triaxial tests

Isotropic consolidated drained and undrained compression triaxial tests (BS 1377-8) were conducted at the Geotechnical Laboratory of the University of Salerno. Each specimen was initially subjected to a filtration stage (starting from the toe towards the top) to evaluate the volume variation and to enhance the initial saturation degree. During this stage, de-aired water was applied under a back pressure of 7 kPa (at the toe) and 5 kPa (at the top) with a confining cell pressure of 12 kPa and a deviator stress of 2 kPa until a clear water flow was observed flowing out from the upper boundary of the specimen (no visible entrapped air bubbles). Then the same back-pressure (7 kPa) was imposed at the two boundaries of the specimens by short-circuiting the two drainage lines initially set independently. The saturation of the specimens was performed by simultaneously increasing the confining cell pressure and the back pressure, keeping the difference between them

at 5 kPa throughout the entire saturation process (Bishop and Henkel 1962). The application of the back pressure from both the bottom and the top of the specimens improved the saturation degree by compressing the air bubbles entrapped between the soil particles. All the samples were finally considered to be saturated for the 200 kPa back pressure, corresponding to a B value equal to 0.95. The height variation of the specimens was recorded continuously by a LVDT during all the test phases.

Consolidated drained and undrained triaxial tests were conducted with effective confining pressures of 10, 30 and 50 kPa. These values can be considered as representative of the in situ confining pressures of soils belonging to superficial layers of pyroclastic deposits. For comparison purposes, both the drained and undrained triaxial tests on the reconstituted bare soils were performed at the same effective consolidation pressures. A consolidation time (t_{100}) equal to 2 hours was derived from the consolidation curve using the Taylor construction in the consolidation plane. According to the BS 1377-8 Standards (BSI 1990), after the consolidation stage, the rate of the axial displacement d_r to apply during the monotonic shear stage was calculated. First, the significant testing time t_f in the compression test was obtained via the product between t_{100} of the consolidation curve and the factor F, which depends on the drainage conditions and the type of compression test to be performed (drained or undrained). The same factor F was selected for both the drained and undrained conditions, considering drainage from both ends of the specimen (F=8.5). An axial strain rate d_r equal to 0.02 mm/min was determined to be related to a significant strain interval of approximately 30%. This last value was the estimated strain ε_f, at which failure will occur for this type of soil (Migliaro 2008). Due to the high compressibility of the tested soil together with the relatively low confining pressures used, a membrane correction was needed to

account for the membrane effect on the inferred deviator stress (Bishop and Henkel 1962) following the expression:

$$(\sigma_1 - \sigma_3) = \frac{F_a}{A} - C_M \quad (1)$$

in which F_a is the measured axial force, A is the section area of the specimen calculated taking into account the geometry variation, and C_M is the correction term that can be calculated as

$$C_M = 4M\epsilon_a \frac{(1-\epsilon_a)}{D} \quad (2)$$

being M the measured extension modulus of the used membrane, $\boldsymbol{\varepsilon}_a$ the axial deformation of the specimen during shear and D the diameter of the specimen at the start of the shear. In our case the measured M modulus was 0.45 N/mm.

During shear, the axial stress, height and volume/pore water pressure variations were recorded. At the end of the test the specimen was weighted. The list of the triaxial tests on both the rooted and bare soil specimens is reported in Table 1. The ID of each sample is composed of 3 characters, referring whether the type of soil is bare or vegetated (B: bare, V: vegetated), the name of the block where it was taken (i.e., A), and the specimen number. Examples of bare soil and root-soil specimens ID are B01 and VA1, respectively.

Root-Soil parameters

The typical structure of the rooted-soil consists of materials in four different phases: solid skeleton, roots, water and air. The soil void ratio e was calculated taking into account the fact that the roots, having a different specific gravity of solid grains, occupy some voids and thus reduce the pore size (Ng et al. 2016; Jotisankasa and Sirirattanachat 2017). The new formula based on this phases' relationship was the following:

$$e = \frac{V_v}{(V_s + V_r)} = \frac{V_{tot} - (V_s + V_r)}{(V_s + V_r)} \quad (3)$$

in which V_v is the volume of the voids, obtained as the difference between the total volume V_{tot} and the volume occupied by the solid grains V_s and roots V_r. This formula was used to calculate the changing in void ratio during the different phases of the triaxial test. The total volume at the end of each phases of the test was back calculated based on the measurement of the water content of the specimen at the end of test and the volume changes measured during consolidation and shearing phases. The root volume (V_r) was calculated as the ratio between the dry root biomass (*RM*) and the root density (γ_r). The *RM* was measured in accordance with the method proposed by Liang et al. (1989). At the end of the triaxial test, each specimen was weighed and oven-dried at 60° C for 24 h. Afterwards, different sieves with a decreasing diameter of the network were used to retain any roots contained in the soil specimen. Furthermore, tweezers were used to remove roots from soil retained at each sieve. A caliper mono-block with an accuracy of 0.05 mm was used to measure the root diameters in order to quantify the distribution frequency of the diameters of the roots grown during the experimental study. Finally, the *RM* and soil mass (*SM*) were weighed.

The procedure adopted for the determination of γ_r was the density bottle method, consisting in the following stages: *i)* 10 g of dry roots were introduced in a pycnometer and weighed (W_2); *ii)* de-aired distilled water was added up to half of the height of the pycnometer and the mixture was boiled to remove air entrapped between the roots; iii) finally the pycnometer was completely filled with de-aired distilled water and the weight and temperature were measured after cooling (W_3). Considering the weight of the dried pycnometer (W_1) and the weight of the pycnometer completely filled with de-aired distilled water (W_4), the root density formula can be obtained:

$$\gamma_r = \frac{RM}{V_r} = \frac{RM}{WM}\gamma_w = \frac{(W_2 - W_1)}{[(W_4 - W_1) - (W_3 - W_2)]}\gamma_w \quad (4)$$

in which *WM* represents the mass of an equivalent volume of water.

In this way, without forcing the saturation of the internal voids of the roots, γ_r was calculated as the average of the γ_r values obtained at the end of three independent experiments. The root density was equal to 6.18 kN/m^3, which is consistent with that provided by Gray and Sotir (1996).

The volume of the soil grain V_s was finally obtained as the ratio between the dry soil mass (*SM*) and the soil density (γ_s). In addition, the Root Volume Density (*RVD*) was calculated (Zhu and Zhang 2016) as the ratio between the total volume occupied by the roots, V_r, (reverting eq. (4)) and the total volume V_{tot} of the root-permeated soil sample at the initial stage, equal to the initial nominal volume of the specimen (D=36.4 mm and H=79.3mm). Therefore:

$$RVD(\%) = \frac{V_r}{V_{tot}} x100 \quad (5)$$

The *RVD* parameter can be considered as the variation of soil porosity due to the presence of roots.

EXPERIMENTAL RESULTS AND DISCUSSIONS

Measured root-soil parameters

The measured root diameters were divided in 4 classes from the lowest (0-0.55 mm) to the highest (1.65-2.20 mm) value measured, comparable with the classification of fine roots provided by Liu et al. (2018). Figure 3a shows the frequency of the root diameters for the samples taken from the superficial zone of the column (Block D). The frequency was calculated as the ratio between the number of roots within the specific diameter class and the total number of roots. The lowest diameter class (0-0.55 mm) showed the maximum frequency, while the highest diameter class (1.65-2.2 mm) showed the minimum frequency. Hence, the grass roots investigated in this experimental study belong to the so-called “fine roots” class, which in the literature are widely recognized to have diameters less than 2 mm (Stokes et al. 2009).

The *RM* and *RVD* values for each root-soil specimen taken from different soil depths of the vegetated column are summarized in Table 2. The measured *RMs* are small for all root-soil specimens if compared with the root mass of shrubs and trees that can have up to 40 kg/m^3 root mass density (ratio between the dry mass of roots and the total volume of the soil) in the top 25 cm of soil (Jackson et al 1996), showing the typical range of values found for grass species. These last usually have reduced quantities of both above and below ground biomass when compared to woody species (Canadell et al. 1996). Moreover they show a decreasing trend with the depth (Fig. 3b). The maximum *RM* measured was equal to 0.16 g, which was from the specimen placed on the upper part of the column investigated in triaxial tests, corresponding to an approximately 200 mm depth from the soil surface. In general, the relatively low *RM* values always found for these grass species can be attributed to their fine and fasciculate root system (Metcalfe and Nelson 1985), which is very light. Our results are consistent with the *RM* measures obtained for other grass species with similar characteristics (Zhu and Zhang 2016).

As expected, the calculated *RVD* values show the same decreasing trend of *RMs* as the depth increases, with a maximum value equal to 0.31% corresponding to the shallowest depth (Table 2), thus highlighting the typical root system of the grass species, which is characterized by numerous fine and light roots.

Behavior in drained conditions

The drained test results on both the bare and vegetated soils are shown in Figure 4 and summarized in Table 1 (test type: D). In all tests during shearing, both the bare and vegetated soil specimens showed a contractive behavior, provided by an increase in the volumetric deformation ε_v ($\Delta V/V$) as the axial strain ε_a ($\Delta H/H$) increased (Fig. 4b, d, f).

Many specimens showed a hardening behavior, being globally flattened as the consolidation pressure increased. Indeed, for a confining pressure of 10 kPa (Fig. 4a, b) the deviator stress increased continuously, as did the volumetric strain. Conversely, the behavior changed for a confining pressure of 50 kPa (Fig. 4e, f). This was due to a reduction of the initial void ratio (densification) before shearing caused by an increase in the consolidation pressure, which improved also the contact between soil particles and roots. From Figure 4 we observed that usually rooted specimens showed an increase in shear strength over the non-rooted samples. For the rooted specimens, as the deformation would be developed roots tend to stop the soil movement by frictional resistance between soil particles and roots, and then part of the soil shear stress is converted into tensile resistance of roots. This increases locally the normal stress with a consequent improvement of shear strength. When soil shear strength is completely developed, only roots can contribute to further increase the global shear resistance of the composite until frictional or tensile resistance of roots is reached. Depending on the initial state of the stress some roots can be broken, thus showing a gradual reduction in shear strength of the rooted soil (Fig. 4c, e).

In the elastic phase of shearing, the axial deformations recorded in the vegetated samples under the same deviator stress were generally lower than those in the bare samples, except for one specimen that showed a higher axial deformation than that of bare soil (Fig. 4c). In general, the presence of roots can increase the stiffness of the composite root-soil system (Fig. 4a, c, e).

The failure conditions were different between the bare and vegetated soil specimens. For example under a confining pressure of 30 kPa (Fig. 4c), the bare soil reached the final conditions for a deviator stress of 85 kPa, while the rooted specimen with the highest percentage of vegetation (VD6), reached a final deviator stress of 120 kPa.

An exception was observed for VC5 specimen (Fig. 4c, d), which, compared to the others vegetated samples, showed a more gradual increment of deviator stress with axial strain, together with a high volumetric deformation. This was because the void ratio of that specimen was larger than that of the other samples tested at the same confining pressure, therefore highlighting an opposite role played by the roots and porosity.

To isolate the role played by the roots on the behavior of the root-soil composite, we attempted to compare both the bare and vegetated samples with a similar void ratio (eq. (3)). From Figure 4e, f, it is possible to observe an increment of the maximum deviator stress as well as a reduction of the volumetric strain as the *RVD* increases. However, the rooted samples were characterized by a high variability in their initial void ratio compared with the 'reference void ratio line' (Fig. 5), which represents the target void ratio used for initially filling the soil column.

Figure 5 shows the initial void ratio after sampling (e_{ini}), the void ratio calculated after filtration (e_{filtr}) and the void ratio after the consolidation stage (e_c) plotted with the *RVD* for all tested specimens. The void ratio values for the bare specimens were those positioned corresponding to *RVD* = 0% on the graph and labelled with their own ID. It is clearly observed that some rooted samples were positioned above the reference line, while others were below it. This variability can be attributed to both the root growth and dry-wetting due to the evapotranspiration-irrigation cycles occurring in the soil column during one vegetative year (Gliński and Lipiec 1990; De León-González et al. 2007). The same variability was also found in the calculated initial bulk density (γ_d). In particular, a value of 11.9±0.03 kN/m^3 was obtained for bare specimens while γ_d of rooted specimens varied within a higher range: 12.1±0.41 kN/m^3. Despite this high variability, all the vegetated specimens generally exhibited a low reduction in the void ratio (hollow squares in Fig. 5a, b, c) during the initial filtration stage compared to the bare specimens. These latter, indeed,

were subjected to a severe particles rearrangement (structural collapse), typical of loose pyroclastic soils (Moscariello et al. 2018), observable by the rapid reduction of the specimens height recorded during the filtration stage. This means that root networks can improve the soil structure stability by providing a support for soil during the saturation processes (i.e., rainfall infiltration). Furthermore, the void ratio values measured after the consolidation process (hollow triangles in Fig. 5a, b, c) were highly reduced in the bare soil compared to the rooted samples.

All results of the drained triaxial tests in terms of the deviator stress and volumetric strain variation at failure vs the *RVD* are plotted in Figure 6. A visible increasing trend of the shear strength with the *RVD* is observed for all applied confining pressures, becoming steeper for the highest *RVD* values measured. Figure 6b highlights that, for all tested specimens, the volumetric deformation due to shear depends on both the presence of roots (*RVD*) and the void ratio at the end of the consolidation process.

For 50 kPa confining pressures, the volume variation showed a clear decreasing trend with the *RVD*, while for 30 kPa it increased as the initial void ratio increased. This combined effect is well explained from the trend demonstrated for 10 kPa consolidated specimens. In this case, the volume strain seems to be independent of the *RVD*, because the more vegetated the sample was, the higher was the void ratio.

It can be claimed that under drained conditions the roots are able to enhance the shear resistance of the composite root-soil system by increasing the maximum deviator stress that the soil can achieve. As for the volumetric deformation, despite contrasting results are obtained due to the influence of porosity on the volumetric behavior of the soil, it is possible to claim that for specimens with similar void ratio the presence of root can reduce the volumetric deformation during shearing.

Behavior in undrained conditions

The undrained test results, obtained in this experimental study for both bare and vegetated soils, are shown in Figs. 7, 8, 9 and summarized in Table 1 (Test type: U). For the bare soils it was observed that upon shearing a drastic increment of pore water pressure occurred, leading to a reduction of the mean effective stress as the axial strain increased. In some cases, the mean effective stress dropped to zero, which is the typical behavior of loose pyroclastic soils involved in the static liquefaction process (Musso and Olivares 2004; Bilotta et al. 2005; Olivares and Damiano 2007).

Figure 7 shows that complete static liquefaction ($\sigma'_3 = 0$) occurred both in bare and in highly porous rooted samples with an initial confining pressure of 10 kPa. For a fair comparison, the rooted specimens with a similar porosity to the bare soils showed an increment of the maximum deviator stress (Fig. 7a) and a small reduction of excess pore water pressure during shearing (Fig. 7c).

At an initial confining pressure of 30 kPa, a complete static liquefaction occurred only for the bare sample. An increment of the maximum deviator stress can be observed (Fig. 8a, b) as can a reduction of the excess pore water pressures (Fig. 8c), as the *RVD* increases. One exception was observed for the rooted specimen with the highest porosity, in which the pore water pressure variation was the highest among the rooted specimens. The rooted specimen with an *RVD* of 0.25% showed a stable behavior. In particular, the root-soil composite tends to assume a dilative-like behavior, confirmed by a small increment of the pore water pressure as long as the failure is approached (Fig. 8c). This trend can also be observed in its positive hardening constitutive behavior (Fig. 8a). Fig. 10 shows images of this last rooted specimen (Fig. 10b) and the bare

control specimen (Fig. 10a) at the end of the undrained shear stage. The final shapes of the specimens are significantly different, even if they both experienced a diffuse failure deformation mode, without the formation of a defined failure plane. In particular, the bare soil liquefied while the vegetated specimen did not liquefy (Fig. 8) because of the light root network created within the porous spaces, as observed in a transversal section of the specimen (Fig. 10c).

For the 50 kPa confining pressure, none of the tested specimens experienced a complete static liquefaction (Fig. 9d). Despite the maximum deviator stress increased for the rooted specimens, a clear influence of the porosity on the shear strength was still found. For specimens with similar void ratio, it is possible to observe a reduction in the pore water pressure generation during the undrained shear stage (Fig. 9c) together with a considerable increment of the shear strength (Fig. 9a) as the *RVD* increases. Conversely, an increment of the initial porosity leads to the highest values of the excess pore water pressures, reflecting into a reduction of the shear resistance.

To analyze the effect of the roots' presence on the undrained behavior of the tested soil, the final excess pore water pressures Δu (i.e., the difference among the pore water pressure and back pressure) vs the *RVD* were plotted in Figure 11 and summarized in Table 1. Generally, the excess pore water pressures were reduced as the *RVD* increased for specimens with similar void ratio and initially consolidated at 30 kPa and 50 kPa. The filled circles also show a qualitative decreasing trend, although the magnitude of the excess pore water pressure was high because of the larger void ratio. For an initial confining pressure of 10 kPa, as already observed in the drained conditions (Fig. 6b), the *RVD* seems to not influence the pore water pressure generation. Indeed, the Δu trend is apparently different from those of the 30 kPa and 50 kPa consolidated specimens. This confirms the antagonistic role played by the *RVD* and the porosity.

As already observed in the drained conditions, the presence of roots tends to reduce the potential volumetric compressibility and thus the pore water pressure generation in the undrained conditions. Furthermore, the roots seem to act as an additional compressible phase to the two already existing phases (water and solid particles). This causes a small volume variation during the undrained compression with a consequent reduction in the build-up pore water pressure. Conversely, the higher the initial porosity, the higher the inhibited volume variation would be, with an increment of generated pore water pressure, which can lead to static liquefaction.

During static liquefaction, the soil element achieves a maximum deviator stress (q_{max}) at a very low strain and then drops down until it reaches a minimum value (q_{min}). Flow failure may occur when the reduction from the peak to the minimum deviator stress is large. The amount of reduction in the undrained shear strength during liquefaction is usually characterized by the undrained brittleness index, I_B (Bishop 1971), as expressed below:

$$I_B = (q_{max}-q_{min})/q_{max} \quad (6)$$

The values of I_B range between 0 and 1, and non-flow or non-brittle behavior can be observed when $I_B = 0$, whereas brittle soil behavior or complete static liquefaction is associated with $I_B = 1$. In some of our performed undrained triaxial tests, the deviator stress decreased after the peak value and then increased at the end of the test (Figs. 7a, 9a). In these cases, the minimum value of the deviator stress, after its drop and before its final increment, is assumed to be q_{min} (Yoshimine et al. 1999).

Figure 12 shows the calculated undrained brittleness index as a function of the *RVD* for all the specimens tested in this study. It can be observed that the bare samples consolidated to 10 kPa and 30 kPa showed liquefaction with $I_B = 0.95$. The I_B values of the rooted specimens decreased with the increment of the *RVD*. The I_B reduction for 10 kPa and 30 kPa consolidated specimens was

steeper than that for the 50 kPa initial confining pressures specimens. For the latter, a non-flow behavior was also observed for the bare specimens. Regardless, it can be asserted that the roots' presence would eventually inhibit the occurrence of static liquefaction. This was also confirmed by the more vegetated specimens under 30 kPa of consolidation pressure, which showed a behavior of switching from brittle to non-brittle (Fig. 8b).

A possible explanation of this behavior is that the roots create a composite system with a structure that is more stable (Boll and Graf 2001) than that usually observed in bare pyroclastic soils. This might be due to the light roots network created within the porous spaces (Fig. 10c), which behaves as a bonding phase between the particles, thus making soil and/or root-soil aggregates (De León-González et al. 2007). This can facilitate the development of tensile stresses in the roots when deformations occur in the soil due to the application of external loads.

Some authors found that this bonding is mostly formed by biological root activities, such as the release of root exudates (Six et al. 2004), organic matter or organic acid that can occur mainly within 2 mm of the roots (Sauer et al. 2006) and consequently alter the entire soil pore structure (Traoré et al. 2000). However, these activities are guaranteed when the plants are alive and, as a consequence, the behavior of root-soil composites showed in these tests can be modified with root decaying.

Shear strength parameters

The observed shear strength of the vegetated soils is higher than that obtained from the bare soil samples, and increases as the *RVD* passes from 0 to 0.3% (Fig. 6a). To the aim of quantifying the shear strength parameters of the composite root-soil system studied, saturated shear envelopes were performed. Since the critical conditions were not always clear for the tested soils because of

the continuous variation of the shear strength and volumetric strain with the deviator stress, a linear regression of *q-p'* points at the end of the failure stages was drawn. Five different envelopes were performed, one for the bare specimens and the remaining for the rooted soil specimens grouped into four *RVD* classes (Fig. 13a).

The Mohr-Coulomb parameters (i.e., Internal friction angle ϕ' and Cohesion C) are related to a and M parameters (in the *q-p'* Cambridge plane) and thus were obtained by the following general equations in the triaxial conditions:

$$\phi' = \arcsin\left(\frac{3 \cdot M}{6 + M}\right); \; C = a \cdot \frac{3 - \sin(\phi')}{6 \cdot \cos(\phi')} \tag{7}$$

All calculated mechanical parameters are summarized in Table 3.

For bare soil, C and ϕ' are properly the effective soil cohesion C_s and the angle of shear resistance of soil particles. Thus, C equals C_s. On the other hand, for vegetated soil the stresses are transferred not only to the soil skeleton but, as in concrete reinforced by steel, to the root-soil reinforced matrix (Thorne 1990). As a consequence, they are more properly defined as integrated parameters. It is generally accepted that the integrated cohesion C takes into account both the soil cohesion and the so-called root cohesion C_r (Burroughs and Thomas 1977; Wu et al. 1979; Waldron and Dakessian 1981; Abe and Ziemer 1991; Sidle 1991; Abernethy and Rutherfurd 2001; Simon and Collison 2002; Pollen 2007; De Baets et al. 2008).

From the test results, the root cohesion C_r for vegetated soils was obtained as the difference between the integrated cohesion C (eq. (5)) and the effective soil cohesion C_s. Figure 13b shows the variation of the integrated mechanical parameters with the *RVD*. It can be observed that the increase in the cohesion due to the roots (C_r) was very small and varied from a minimum of 0.4 kPa up to a maximum of 2.1 kPa as the *RVD* increased. The highest root cohesion was obtained for samples with the highest *RVD* value.

The integrated friction angle ϕ' also increased with the *RVD* up to a maximum value of 40 degrees. In our case, the resistance contribution due to the tensile strength of the fibers intersecting the failure plane was very limited, because of the diffused failure deformation mode observed for all the tested specimens (i.e., without any formation of a well-defined shear plane). In fact, the ductile behavior of the samples was evidenced by the increase in specimen diameter as the axial strain increase. The maximum extension occurred in the horizontal plane and thus the roots orientated in this direction were those that mostly contributed to the soil strength. This failure mechanism led the horizontal roots to be stretched causing tensile stress to be induced, enhancing the stabilizing horizontal external forces acting on the unstable soil volume. This mechanism enhanced the shear resistance of the root-soil composite. Hence, it is possible to argue that roots mostly provide a stress dependent contribution on the shear resistance of the composite material. These insights are consistent with the results of triaxial tests conducted on low density soils vegetated with *Alnus incana* species directly planted in the specimen (Graf et al. 2009) as well as on reconstituted specimens with roots geometrically distributed inside the soil (Zhang et al. 2010).

In conclusion, the volume percentage occupied by the roots of *graminae* grass species in a sample can indirectly indicate the complexity of the roots network, which influences the behavior of the whole structure. Indeed, the *RVD* increment improves the interaction between the roots and soil due to the higher complexity of the root-soil system, enhancing the shear strength parameters.

CONCLUSIONS

The triaxial test results on bare and rooted specimens allow to quantify the characteristics of the roots *graminae* network growing in pyroclastic soils as follows.

The perennial *graminae* grasses are easily able to grow in pyroclastic soils within one vegetative year by developing a light root network up to 2 meters in depth and with a mean root diameter of 0.55 mm. According to other authors, the distribution of the *RM*, and consequently the *RVD*, decreases with depth.

In the consolidated triaxial tests under drained conditions, the volumetric deformations in the rooted soils are reduced and the maximum deviator stress increases as the percentage of the root volume within the soil (*RVD*) increases. Furthermore, a positive correlation of the shear strength parameters with the *RVD* was found. Since in our case the integrated friction angle (ϕ') is the most affected parameter, a stress-dependent contribution of the roots on the shear resistance can be proven. Moreover, considering the decreasing trend of the roots volume with depth, we can also suppose the same trend for the mechanical parameters.

The consolidated undrained triaxial tests show the most interesting results since the roots reduced the pore water pressure generation during shearing as the *RVD* in soil increased. Furthermore, the brittleness index I_B for the vegetated soils generally had lower results than unity (I_B = 1, corresponding to static liquefaction), highlighting that the roots reduce the probability of the static liquefaction occurrence for most of the rooted specimens. Indeed, the vegetated soil behaved similar to a composite, in which the stresses were distributed between the solid skeleton and the root network, reducing the potential volume variation. In one specific case, dilative-like behavior (switching from brittle to non-brittle) was observed. Nevertheless, these results were affected by the void ratio variability of the specimens, stressing the antagonistic role played by the porosity and the root volume density.

In conclusion, the experimental results strongly encourage further laboratory and in situ investigations in order to approve of the fine roots of the *graminae* grass species as a stabilization

measure of pyroclastic soils suffering collapse and liquefaction in undrained conditions after the first failure stage. For this purpose, knowledge improvement must be addressed on the rheology of material testing specimens at a wider range of porosity and *RVD* values. Furthermore, investigations into when roots decay must be conducted in order to assess the potential role of this sustainable bio-engineering practice in the long term.

ACKNOWLEDGMENTS

The authors are grateful to the Editor-in-Chief, Daichao Sheng, and to the two anonymous referees for their useful and fruitful comments and suggestions.

The experimental tests reported in this work have been performed during the PhD research of Capobianco V. at the University of Salerno. The authors would like to acknowledge the Prati Armati S.r.l. for having provided the seeds of the grass species for the experimental study.

The authors also wish to thank the Norwegian Geotechnical Institute for hosting part of the research period of the Post Doc Vittoria Capobianco within *WP3.2 Mitigation measures* in the Research Council of Norway funded Klima 2050 project.

REFERENCES

ASTM 2010. Standard practice for classification of soils for engineering purposes (Unified Soil Classification System). West Conshohocken, PA, USA: ASTM International.

Bilotta, E., Cascini, L., Foresta, V., and Sorbino, G. 2005. Geotechnical characterisation of pyroclastic soils involved in huge flow slides. Geotechnical & Geological Engineering, **23**(4): 365–402.

Bilotta, E., Foresta, V., and Migliaro, G. 2006. Suction controlled laboratory tests on undisturbed pyroclastic soil: stiffnesses and volumetric deformations. *In* Proceedings of the Fourth International Conference on Unsaturated Soils, UNSAT, Carefree, Arizona, UNSAT, 2-6 April 2006. American Society of Civil Engineers, pp. 849–860.

Bilotta, E., Foresta, V., and Migliaro, G. 2008. The influence of suction on stiffness, viscosity and collapse of some volcanic ashy soils. *In* Proceedings of the First European Conference on Unsaturated Soils, E-UNSAT, Durham, United Kingdom, 2-4 July 2008. CRC Press, Vol. 1, pp. 349–354.

Bishop, A., W., and Henkel, D. J. 1962. The measurement of soil properties in the triaxial test. Edward Arnold (Publishers), London, UK.

Bishop, A.W. 1971. Shear Strength Parameters for Undisturbed and Remoulded Soil Specimens. *In* Proceedings of the Roscoe Memorial Symposium, Cambridge University, Cambridge, Mass, pp. 3–58.

Böll, A., and Graf, F. 2001. Nachweis von Vegetationswirkungen bei oberflächennahen Bodenbewegungen - Grundlagen eines neuen Ansatzes. Schweiz. Z. Forstwes. 152: 1-11.

Bonneu, A., Dumont, Y., Rey, H., Jourdan, C., and Fourcaud, T. 2012. A minimal continuous model for simulating growth and development of plant root systems. Plant and soil, **354**(1-2): 211-227.

British Standards Institution 1990. Method of test for soils for civil engineering purposes. Shear stretch tests (effective stress), BS 1377-8: 1990. Milton Keynes: BSI.

Campbell, R. H. 1975. Soil slips, debris flows, and rainstorms in the Santa Monica Mountains and vicinity, southern California. US Geological Survey, Professional Paper 851, 51.

Canadell, J., Jackson, R. B., Ehleringer, J. B., Mooney, H. A., Sala, O. E., and Schulze, E. D. 1996. Maximum rooting depth of vegetation types at the global scale. Oecologia, **108**(4): 583-595.

Capra, L., Lugo-Hubp, J., and Borselli, L. 2003. Mass movements in tropical volcanic terrains: the case of Teziutlán (México). Engineering Geology, **69**(3): 359–379.

Cascini, L., Cuomo, S., and Della Sala, M. 2011. Spatial and temporal occurrence of rainfall-induced shallow landslides of flow type: A case of Sarno-Quindici, Italy. Geomorphology, **126**(1-2): 148–158.

Cascini, L., Cuomo, S., Pastor, M., and Sorbino, G. 2010. Modeling of rainfall-induced shallow landslides of the flow-type. Journal of Geotechnical and Geoenvironmental Engineering, **136**(1): 85–98.

Cascini, L., Guida, D., Nocera, N., Romanzi, G., and Sorbino, G. 2000. A preliminary model for the landslides of May 1998 in Campania Region. *In* Proceedings of the 2nd International Symposium on Geotechnics of Hard Soil-Soft Rock, Balkema, Napoli, Vol. 3, pp. 1623–1649.

Cazzuffi, D., Corneo, A., and Crippa, E. 2006. Slope stabilisation by perennial "gramineae" in southern Italy: plant growth and temporal performance. Geotechnical and Geological Engineering, **24**(3): 429–447.

Celico, P., Guadagno, F. M., and Vallario, A. 1986. Proposta di un modello interpretativo per lo studio delle frane nei terreni piroclastici. Geologia Applicata e Idrogeologia, XXI, 173–193.

Chu, J., Leroueil, S., and Leong, W. K. 2003. Unstable behaviour of sand and its implications for slope instability. Canadian Geotechnical Journal, **40**(5): 873–885.

Cioni, R., Santacroce, R., and Sbrana, A. 1999. Pyroclastic deposits as a guide for reconstructing the multi-stage evolution of the Somma-Vesuvius Caldera. Bulletin of Volcanology, **61**(4): 207–222.

Comino, E., and Druetta, A. 2010. The effect of Poaceae roots on the shear strength of soils in the Italian alpine environment. Soil and Tillage Research, **106**(2): 194-201.

De León-González, F., Gutiérrez-Castorena, M.C., González-Chávez, M.C.A., and Castillo-Juárez, H. 2007. Root-aggregation in a pumiceous sandy soil. Geoderma **142**: 308-317.

Del Prete, M., Guadagno, F. M., and Hawkins, A. B. 1998. Preliminary report on the landslides of 5 May 1998, Campania, southern Italy. Bulletin of Engineering Geology and the Environment, **57**(2): 113–129.

De Vita, P., Agrello, D., and Ambrosino, F. 2006a. Landslide susceptibility assessment in ash-fall pyroclastic deposits surrounding Mount Somma-Vesuvius: Application of geophysical surveys for soil thickness mapping. Journal of Applied Geophysics, **59**(2): 126–139.

Eckersley, D. 1990. Instrumented laboratory flowslides. Geotechnique, **40**(3): 489–502.

Eisenhauer, N., Beßler, H., Engels, C., Gleixner, G., Habekost, M., Milcu, A., and Weigelt, A. 2010. Plant diversity effects on soil microorganisms support the singular hypothesis. Ecology, **91**(2): 485–496.

Endo, T., and Tsuruta, T. 1969. The effect of the tree's roots on the shear strength of soil, Annual Report of the Hokkaido Branch Forest Experiment Station, Sapporo, Japan, pp. 167–182.

Ferlisi, S., De Chiara, G., and Cascini, L. 2016. Quantitative risk analysis for hyperconcentrated flows in Nocera Inferiore (southern Italy). Natural Hazards, **81**(1): 89–115.

Fiorillo, F., Guadagno, F., Aquino, S., and De Blasio, A. 2001. The December 1999 Cervinara landslides: further debris flows in the pyroclastic deposits of Campania (southern Italy). Bulletin of Engineering Geology and the Environment, **60**(3): 171–184.

Frei, M. 2009. Validation of a new approach to determine vegetation effects on superficial soil movements. Ph.D. thesis, ETH Zurich.

Gliński, J., and Lipiec, J. 1990. Soil Physical Conditions and Plant Roots. CRC Press Inc., Boca Raton Florida.

Graf, F., Frei, M., and Böll, A. 2009. Effects of vegetation on the angle of internal friction of a moraine. Forest Snow and Landscape Research, **82**(1): 61–77.

Gray, D. H., and Sotir, R. B. 1996. Biotechnical and soil bioengineering slope stabilization: a practical guide for erosion control. John Wiley & Sons Inc.

Guadagno, F. M. 2000. The landslides of 5th May 1998 in Campania, Southern Italy: natural disasters or also man-induced phenomena. Journal of Nepal geological society, **22**: 181–187.

Guadagno, F. M., and Revellino, P. 2005. Debris avalanches and debris flows of the Campania Region (southern Italy). *In* Debris-flow Hazards and Related Phenomena. Springer Berlin Heidelberg, Chapter 19, pp. 489–518.

Hungr, O., Evans, S. G., and Hutchinson, I. 2001. A Review of the Classification of Landslides of the Flow Type. Environmental & Engineering Geoscience. **7**(3): 221–238.

Hu, X. S., Brierley, G., Zhu, H. L., Li, G. R., Fu, J. T., Mao, X. Q., and Qiao, N. 2013. An exploratory analysis of vegetation strategies to reduce shallow landslide activity on loess hillslopes, Northeast Qinghai-Tibet Plateau, China. Journal of Mountain Science, **10**(4), 668–686.

Iverson, R. M., Reid, M. E., and LaHusen, R. G. 1997. Debris-flow mobilization from landslides. Annual Review of Earth and Planetary Sciences, **25**(1): 85–138.

Jackson, R. B., Canadell, J., Ehleringer, J. R., Mooney, H. A., Sala, O. E., and Schulze, E. D. 1996. A global analysis of root distributions for terrestrial biomes. Oecologia, **108**(3): 389–411.

Jastrow, J. D., Miller, R. M., and Lussenhop, J. 1998. Contributions of interacting biological mechanisms to soil aggregate stabilization in restored prairie. Soil Biology and Biochemistry, **30**(7): 905–916.

Jotisankasa, A., and Sirirattanachat, T. 2017. Effects of grass roots on soil-water retention curve and permeability function. Canadian Geotechnical Journal, **54**(11): 1612–1622.

Keefer, D. K., and Larsen, M. C. 2007. Assessing landslide hazards. Science, **316**(5828): 1136–1138.

Ladd, R. S. 1977. Specimen preparation and cyclic stability of sands. Journal of Geotechnical and Geoenvironmental Engineering, (ASCE 13014 Proceeding), **103**: 535–547.

Lancellotta, R., Di Prisco, C., Costanzo, D., Foti, S., Sorbino, G., Buscarnera, G., Cosentini, R.M., and Foresta, V. 2012. Caratterizzazione e modellazione geotecnica. *In* Criteri di zonazione della suscettibilità e della pericolosità da frane innescate da eventi estremi (piogge e sisma)/Leonardo Cascini. Composervice srl, Padova, pp. 266–319. ISBN 9788890687334.

Leung, F. T., Yan, W. M., Hau, B. C., and Tham, L. G. 2015a. Root systems of native shrubs and trees in Hong Kong and their effects on enhancing slope stability. Catena, **125**: 102–110.

Liang, Y. M., Hazlett, D. L. and Lauenroth, W. K. 1989. Biomass dynamics and water use efficiencies of five plant communities in the shortgrass steppe. Oecologia, **80**(2): 148–153.

Lim, T. T., Rahardjo, H., Chang, M. F., and Fredlund, D. G. 1996. Effect of rainfall on matric suctions in a residual soil slope. Canadian Geotechnical Journal, **33**(4): 618–628.

Lirer, L., Petrosino, P., Alberico, I., and Postiglione, I. 2001. Long-term volcanic hazard forecasts based on Somma-Vesuvio past eruptive activity. Bulletin of volcanology, **63**(1): 45–60.

Liu, K., Yang, X., Xie,X., Wu, C., and Liu, Y. 2011. Laboratory Triaxial Test Study on Soil Reinforce with Roots of Manilagrass. Advanced Materials Research, **250**(253):1366–1370.

Liu, Y., Wang, G., Yu, K., Li, P., Xiao, L., and Liu, G. 2018. A new method to optimize root order classification based on the diameter interval of fine root. Scientific reports, **8**(1): 2960.

Mastrolorenzo, G., Palladino, D. M., Vecchio, G., and Taddeucci, J. 2002. The 472 AD Pollena eruption of Somma-Vesuvius (Italy) and its environmental impact at the end of the Roman Empire. Journal of Volcanology and Geothermal Research, **113**(1-2): 19–36.

Meisina, C. 2006. Characterisation of weathered clayey soils responsible for shallow landslides. Natural Hazards and Earth System Science, **6**(5): 825–838.

Metcalfe, D. S., and Nelson, C. J. 1985. The botany of grasses and legumes. Forages: The science of grassland agriculture. M.E. Heath et al. Iowa State University Press: Ames, pp. 52–63.

Migliaro, G. 2005. Il legame costitutivo dei terreni piroclastici per la modellazione di scavi in ambiente urbanizzato ed influenza della parziale saturazione. Ph.D. Thesis, Department of Civil Engineering, University of Salerno, Italy.

Moscariello, M., Cuomo, S., and Salager, S. 2018. Capillary collapse of loose pyroclastic unsaturated sands characterized at grain scale. Acta Geotechnica, **13**: 117-133.

Musso, A., and Olivares, L. 2004. Post-failure evolution in flow-slide: Transition from static liquefaction to fluidization. *In* Proceedings of the International Workshop on Occurrence and Mechanisms of Flow-Like Landslides in Natural Slopes and Earthfills, Sorrento, Italy, pp. 117–128.

Ng, C. W. W., Leung, A. K., and Woon, K. X. 2013. Effects of soil density on grass-induced suction distributions in compacted soil subjected to rainfall. Canadian Geotechnical Journal, **51**(3): 311–321.

Ng, C. W. W., Ni, J. J., Leung, A. K., and Wang, Z. J. 2016. A new and simple water retention model for root-permeated soils. Géotechnique Letters, **6**(1): 106–111.

Ng, C. W. W., Ni, J. J., Leung, A. K., Zhou, C. and Wang, Z. J. 2016. Effects of planting density on tree growth and induced soil suction. Géotechnique, **66**(9), 711–724.

Ng, C.W.W., Tasnim, R., Capobianco, V. and Coo, J.L. 2018. Influence of soil nutrients on plant characteristics and soil hydrological responses. Géotechnique Letters **8**(1), 19-24.

Ni, J.J., Leung, A.K., Ng, C.W.W. and Shao, W. 2018. Modelling hydro-mechanical reinforcements of plants to slope stability. Computers and Geotechnics **95**, 99-109.

Nicotera, M. V. 1998. Effetti del grado di saturazione sul comportamento di una pozzolana del napoletano. Ph.D. Thesis, Università di Napoli Federico II, Italy.

Nilaweera, N. S. 1994. Effects of tree roots on slope stability-The case of Khao Lunag Mountain Area, Southern Thailand. Ph.D. Thesis No. GT-93-2, Bangkok, Asian Institute of Technology.

Nilaweera, N. S., and Nutalaya, P. 1999. Role of tree roots in slope stabilisation. Bulletin of Engineering Geology and the Environment, **57**(4): 337–342.

Olivares, L., and Damiano, E. 2007. Postfailure mechanics of landslides: laboratory investigation of flowslides in pyroclastic soils. Journal of Geotechnical and Geoenvironmental Engineering, **133**(1): 51–62.

Operstein, V., and Frydman, S.2000. The influence of vegetation on soil strength. Proceedings of the Institution of Civil Engineers - Ground Improvement, **4**(2): 81–89.

Pierson, T. C. 2005. Hyperconcentrated flow-transitional process between water flow and debris flow. *In* Debris-flow hazards and related phenomena, Springer Berlin Heidelberg, pp. 159–202.

Pirone, M., Papa, R., Nicotera, M. V., and Urciuoli, G. 2015. In situ monitoring of the groundwater field in an unsaturated pyroclastic slope for slope stability evaluation. Landslides, **12**(2): 259–276.

Reid, M. E., Nielsen, H. P., and Dreiss, S. J. 1988. Hydrologic factors triggering a shallow hillslope failure. Bulletin of the Association of Engineering Geologists, **25**(3): 349–361.

Revellino, P., Hungr, O., Guadagno, F. M., and Evans, S. G. 2004. Velocity and runout simulation of destructive debris flows and debris avalanches in pyroclastic deposits, Campania region, Italy. Environmental Geology, **45**(3): 295–311.

Sauer, D., Kuzyakov, Y., and Stahr, K. 2006. Spatial distribution of root exudates of five plant species as assessed by ^{14}C labeling. Journal of Plant Nutrition and Soil Science, **169**(3): 360–362.

Sidle, R. C., and Ochiai, H. 2006. Landslides: processes, prediction, and land use. Water resources monograph series. Natural Resources Forum, **31**: 322-326.

Six, J., Bossuyt, H., Degryze, S., and Denef, K. 2004. A history of research on the link between (micro) aggregates, soil biota, and soil organic matter dynamics. Soil and Tillage Research, **79**(1): 7–31.

Stokes, A., Atger, C., Bengough, A. G., Fourcaud, T., and Sidle, R. C. 2009. Desirable plant root traits for protecting natural and engineered slopes against landslides. Plant and Soil **324**(1-2): 1–30.

Thorne, C.R. 1990. Effects of vegetation on riverbank erosion and stability. *In* Vegetation and Erosion. *Edited by* J.B. Thornes, John Wiley and Sons Inc., Chichester, pp. 125–143.

Tobias, S. 1995. Shear strength of the soil root bond system. *In* Vegetation and Slopes. *Edited by* Thomas Telford, London, pp. 280–286.

Toll, D. G., Rahardjo, H., and Leong, E. C. 1999. Land-slides in Singapore. *In* Proceedings of the 2nd International Conference on Landslides, Slope Stability and the Safety of Infra-Structures, Singapore, 27-28 July 1999, pp. 27–28.

Traoré, O., Groleau-Renaud, V., Plantureux, S., Tubeileh, A., and Boeuf-Tremblay, V. 2000. Effect of root mucilage and modelled root exudates on soil structure. European journal of Soil Science, **51**(4): 575–581.

Trustrum, N. A., Gomez, B., Page, M. J., Reid, L. M., and Hicks, D. M. 1999. Sediment production and output: The relative role of large magnitude events in steepland catchments. Zeitschrift für Geomorphologie Supplement Volumes, 71–86.

Van Asch, T. W., Malet, J. P., and Van Beek, L. P. H. 2006. Influence of landslide geometry and kinematic deformation to describe the liquefaction of landslides: some theoretical considerations. Engineering geology, **88**(1): 59–69.

Waldron, L. J. 1977. The shear resistance of root-permeated homogeneous and stratified soil. Soil Science Society of America Journal, **41**(5): 843–849.

Wang, F. W., Sassa, K., and Wang, G. 2002. Mechanism of a long-runout landslide triggered by the August 1998 heavy rainfall in Fukushima Prefecture, Japan. Engineering Geology, **63**(1): 169–185.

Wu, T. H. 2013. Root reinforcement of soil: review of analytical models, test results, and applications to design. Canadian Geotechnical Journal, **50**(3): 259–274.

Wu, T. H., Bettadapura, D. P., and Beal, P. E. 1988. A statistical model of root geometry. Forest Science, **34**(4): 980–997.

Wu, T. H., McKinnell III, W. P., and Swanston, D. N. 1979. Strength of tree roots and landslides on Prince of Wales Is-land, Alaska. Canadian Geotechnical Journal, **16**(1): 19–33.

Wu, T. H., and Watson, A. 1998. In situ shear tests of soil blocks with roots. Canadian Geotechnical Journal, **35**(4): 579–590.

Yildiz, A., Graf, F., Rickli, C., and Springman, S. M. 2018. Determination of the shearing behaviour of root-permeated soils with a large-scale direct shear apparatus. Catena, **166**: 98-113.

Yoshimine, M., Robertson, P.K., and Wride, C.E. 1999. Undrained shear strength of clean sands to trigger flow liquefaction. Canadian Geotechnical Journal, **36**: 891–906.

Zhang, C. B., Chen, L. H., Liu, Y. P., Ji, X. D., and Liu, X. P. 2010. Triaxial compression test of soil–root composites to evaluate influence of roots on soil shear strength. Ecological Engineering, **36**(1): 19–26.

Zhu, H., and Zhang, L. M. 2016. Field investigation of erosion resistance of common grass species for soil bioengineering in Hong Kong. Acta Geotechnica, **11**(5): 1047–1059.

Ziemer, R.R. 1981. Roots and the stability of forested slopes. *In* Erosion and sediment transport in Pacific Rim Steeplands. Pub. No. 132. International Association of Hydrological Sciences, pp. 343–361.

Table 1. Details of triaxial compression tests.

ID sample	Type	p'_c kPa	e_{ini}	e_{filtr}	e_c	e_{fin}	p'_{fin} kPa	q_{fin} kPa	RVD %	Δu kPa	$\Delta\varepsilon_v$
B01	D	10	1.170	1.003	1.001	0.934	10.5	13.2	0.00	-	0.036
VB5	D	10	1.065	1.077	1.069	0.999	17.6	22.4	0.12	-	0.036
VC6	D	10	1.182	1.177	1.197	1.104	23.5	41.7	0.27	-	0.042
VD5	D	10	1.188	1.176	1.181	1.091	29.0	54.3	0.31	-	0.041
B02	D	30	1.171	0.989	0.905	0.860	60.3	84.7	0.00	-	0.042
VA5	D	30	1.088	1.091	1.056	1.039	55.9	78.0	0.08	-	0.013
VB6	D	30	1.226	1.206	1.186	1.150	59.4	87.6	0.10	-	0.017
VC5	D	30	1.283	1.274	1.250	1.111	63.6	98.0	0.23	-	0.062
VD6	D	30	1.098	1.088	1.051	1.005	69.9	119.6	0.29	-	0.022
B03	D	50	1.172	1.061	0.949	0.905	83.9	121.4	0.00	-	0.029
VA4	D	50	1.070	1.089	1.030	0.995	98.2	145.4	0.15	-	0.017
VD4	D	50	1.093	1.084	0.996	0.966	108.8	177.1	0.19	-	0.015
B04	U	10	1.162	1.122	1.104	1.104	0.2	0.3	0.00	8.4	-
VB3	U	10	1.134	1.123	1.130	1.130	7.0	10.9	0.13	7.2	-
VC3	U	10	1.257	1.251	1.248	1.248	0.5	0.5	0.15	9.9	-
VD3	U	10	1.192	1.199	1.188	1.188	5.4	12.7	0.29	9.7	-
B05	U	30	1.170	1.113	1.015	1.015	0.3	0.7	0.00	28.4	-
VB2	U	30	1.057	1.069	1.011	1.011	26.7	41.5	0.13	17.6	-
VC2	U	30	1.130	1.130	1.081	1.081	13.6	21.2	0.17	24.9	-
VD2	U	30	1.052	1.034	1.012	1.012	48.6	84.1	0.25	10.7	-
B06	U	50	1.175	1.041	0.946	0.946	20.3	26.0	0.00	38.9	-
VA1	U	50	1.111	1.108	1.058	1.058	42.4	64.0	0.17	29.4	-
VB1	U	50	1.015	1.018	0.978	0.978	52.2	81.6	0.23	26.1	-
VC1	U	50	1.276	1.273	1.180	1.180	12.9	18.1	0.12	45.1	-
VD1	U	50	1.196	1.191	1.140	1.140	32.4	58.9	0.19	38.7	-

Type D = drained test; Type U = undrained test; p'_c = mean effective consolidation stress; e_{ini} = void ratio after the sampling; e_{filtr} = void ratio at the end of filtration stage; e_c = void ratio after consolidation; e_{fin} = void ratio at failure; p'_{fin} = mean effective stress at failure; q_{fin} = deviator stress at failure; RVD = root volume density; Δu = excess pore water pressure at failure; $\Delta\varepsilon_v$ = volume strain variation at failure.

Table 2. Root parameters measured for each root-soil specimen of triaxial tests.

column zone	depth m	ID sample	RM g	average RM g	SD RM g	average RVD %	SD RVD %
A	1.515	VA1	0.09	0.07	0.02	0.13	0.04
		VA4	0.08				
		VA5	0.04				
B	1.115	VB2	0.07	0.06	0.01	0.12	0.02
		VB3	0.07				
		VB6	0.05				
	1.015	VB1	0.12	0.09	0.03	0.17	0.06
		VB5	0.06				
C	0.515	VC2	0.09	0.12	0.03	0.22	0.05
		VC6	0.14				
	0.415	VC1	0.06	0.09	0.02	0.17	0.05
		VC3	0.08				
		VC5	0.12				
D	0.315	VD2	0.13	0.13	0.02	0.24	0.04
		VD4	0.10				
		VD6	0.15				
	0.215	VD1	0.10	0.14	0.03	0.26	0.05
		VD3	0.15				
		VD5	0.16				

RM = Root dry mass; average RM = Average Root dry mass; SD RM = Standard Deviation of Root dry mass; average RVD = Average Root Volume Density; SD RVD = Standard Deviation of Root Volume density.

Table 3. Details of parameters at failure stage for vegetated soils grouped in RVD classes and bare specimens.

group	a kPa	M	C_r kPa	ϕ' °	average RVD %	SD RVD %
Bare	0.0	1.4	0.0	35.2	0	0
Gr1	0.0	1.4	0.0	35.2	0.10	0.02
Gr2	0.8	1.5	0.4	36.4	0.15	0.02
Gr3	2.5	1.6	1.3	38.7	0.21	0.02
Gr4	4.1	1.7	2.1	40.4	0.28	0.02

a = intercept of the failure envelope in *q-p'* plane; M = slope of failure envelope in *q-p'* plane; C_r = Root cohesion; ϕ' = integrated friction angle; average RVD = Average Root Volume Density; SD RVD = Standard Deviation of Root Volume density.

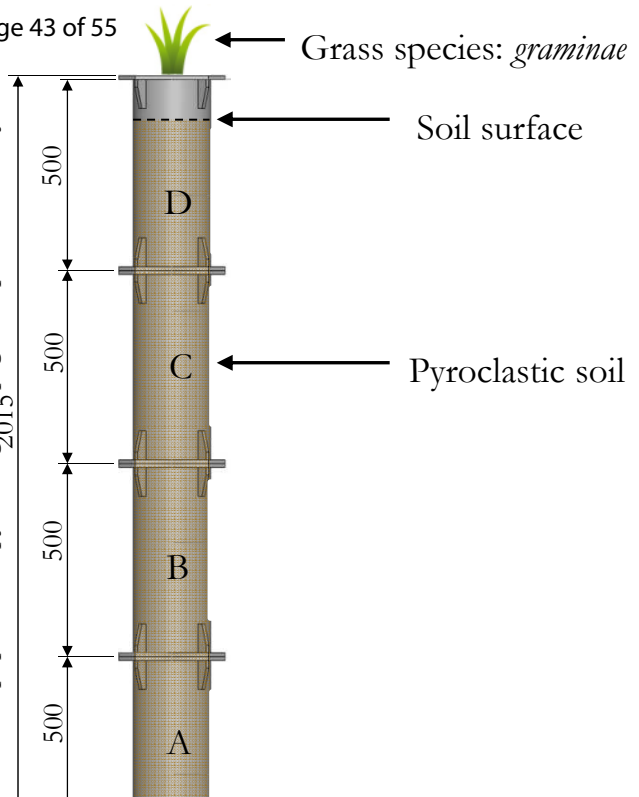

Figure 1. Schematization of experimental set-up of vegetated column: frontal view. All dimensions are in mm.

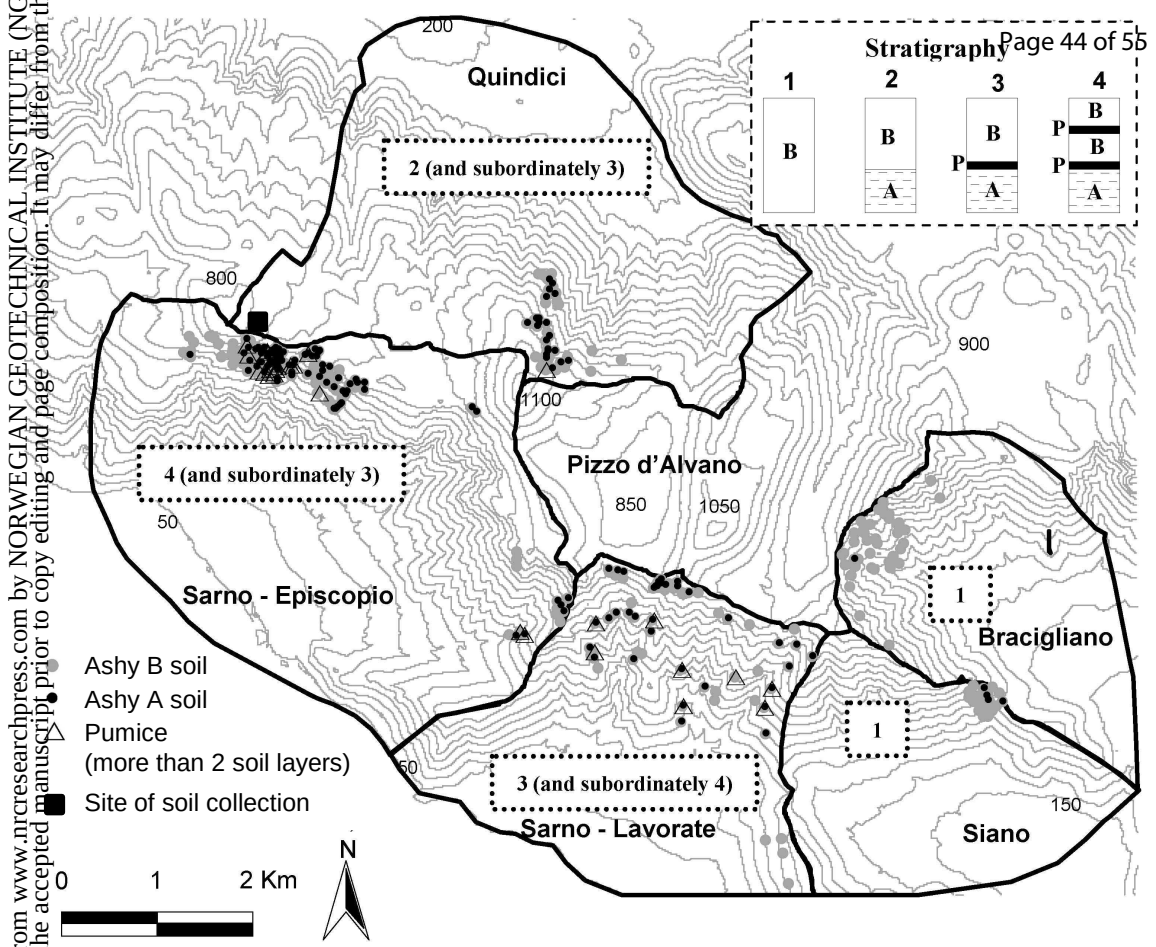

Figure 2. Overview of the five-sector zones affected by flow-like mass movements in the May 1998 with indication of typical stratigraphy type, main litotypes (Bilotta et al. 2005) and its spatial distribution; the dashed square point represents the site where material was collected, in Tuostolo basin, close to the source area of the Tuostolo debris flow (on the left side of the square). (Cascini et al. 2011 modified).

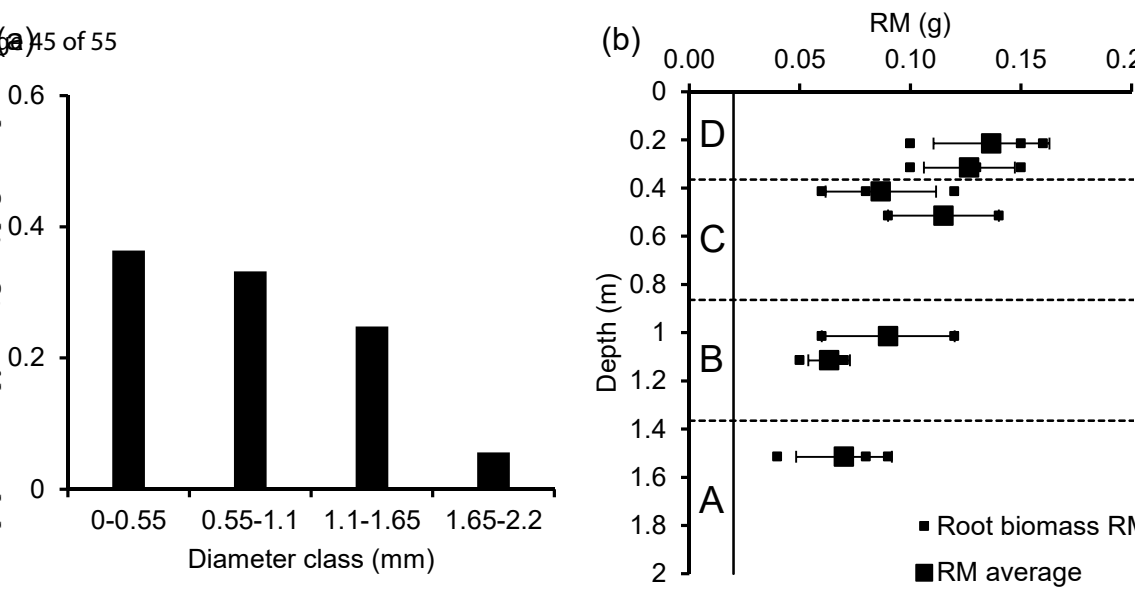

Figure 3. (a) Frequency of measured root diameters divided in four classes for rooted specimens taken from the shallowest block of the soil column; (b) Individual and average Root dry biomass *RM* of triaxial specimens vs sampling depth.

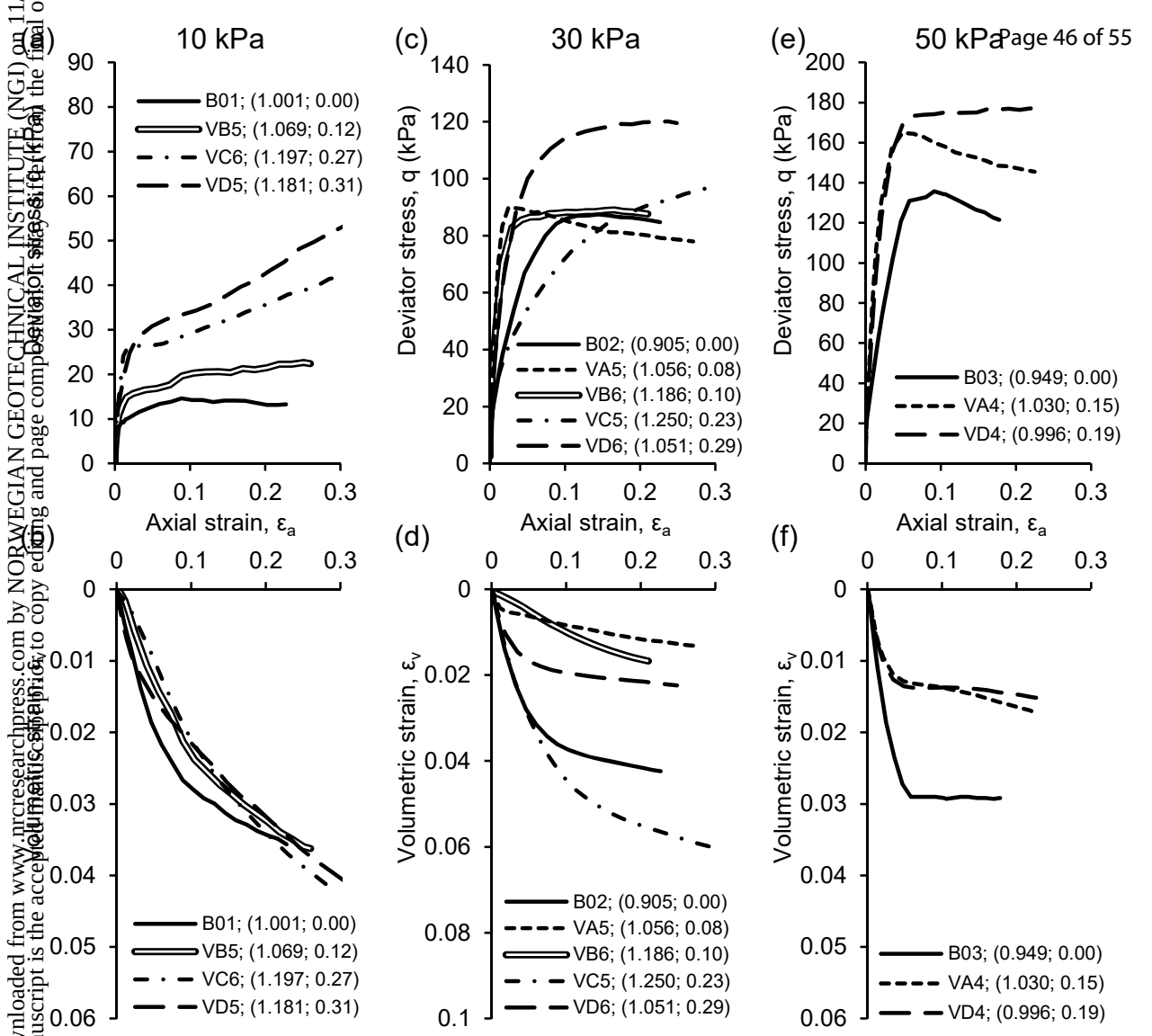

Figure 4. Drained triaxial test results in terms of deviator stress ($q = \sigma_1 - \sigma_3$) vs axial strain ($\varepsilon_a = \Delta H/H$) and volumetric strain ($\varepsilon_v = \Delta V/V$) vs axial strain for: (a, b) 10 kPa, (c, d) 30 kPa and (e, f) 50 kPa confining pressures. For each specimen the void ratio e_c and the *RVD* value are reported in brackets.

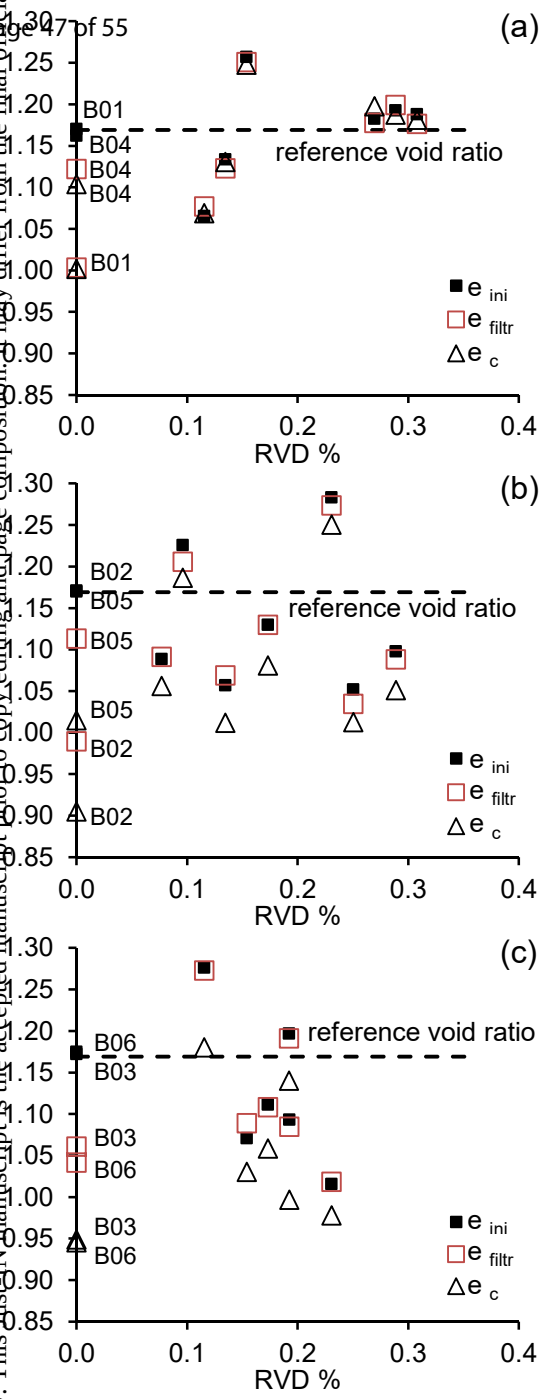

Figure 5. Calculated Void ratio values for each tested specimen respectively at (a) 10 kPa, (b) 30 kPa and (c) 50 kPa consolidation pressures; e_{ini} = initial void ratio at the beginning of the test, e_{filtr} = void ratio at the end of the saturation stage, e_{c} = void ratio at the end of the consolidation stage, reference void ratio = target void ratio of the soil column.

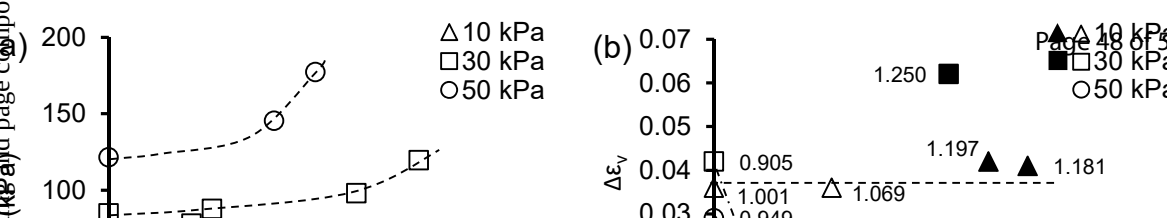

Figure 6. (a) Final deviator stress (q_f) vs *RVD* for 10kPa, 30 kPa and 50 kPa confining pressures; (b) Total volumetric strain variation ($\Delta\varepsilon_v$) vs *RVD* for 10, 30 and 50 kPa confining pressures. Labels represent the void ratio e_c, filled symbols correspond to specimens showing an anomalous trend.

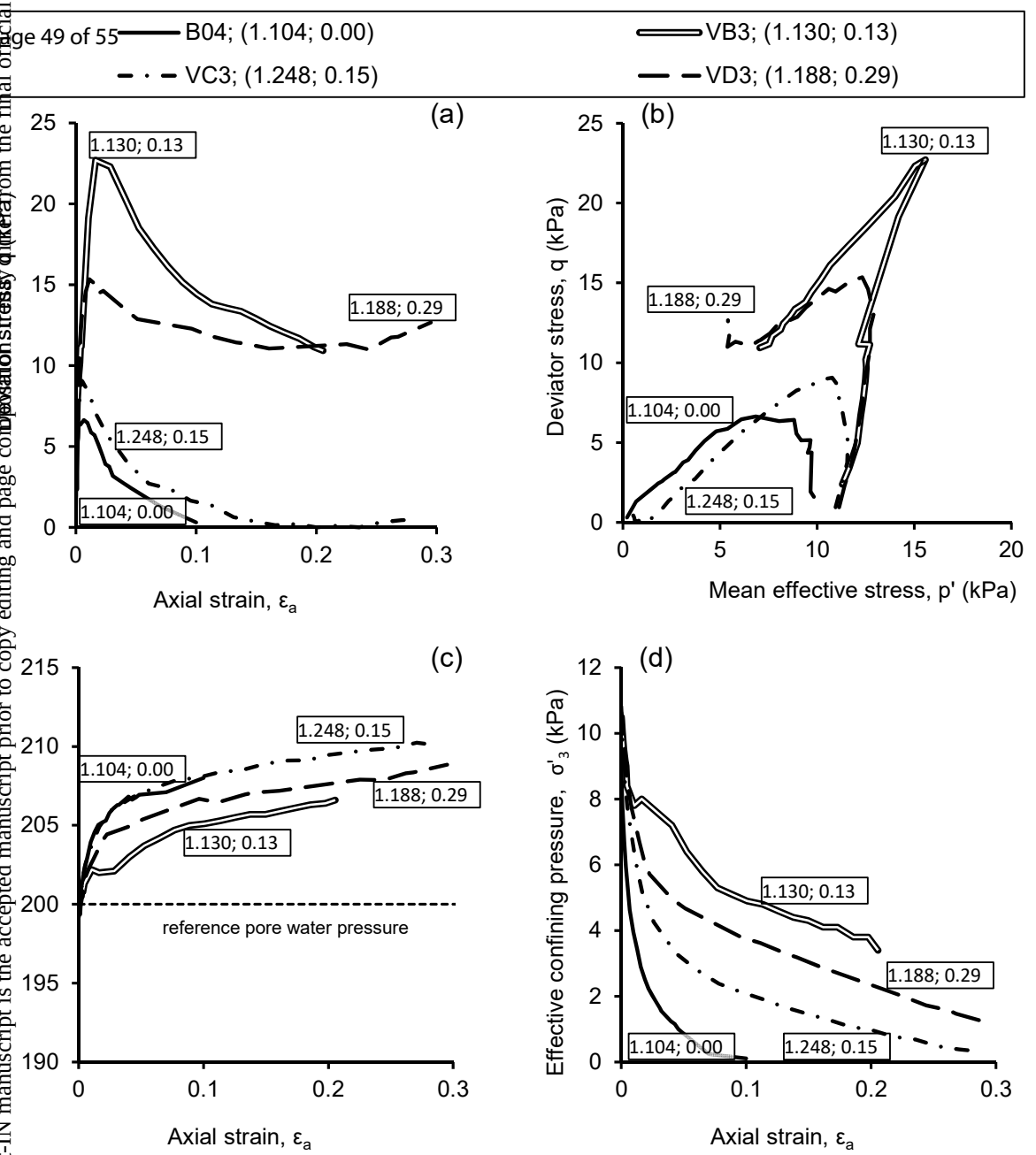

Figure 7. (a) Deviator stress (q_f) vs axial strain (ε_a); (b) Effective stress path in the Cambridge plane (q-p'); (c) Pore water pressure variation vs axial strain and (d) Effective confining pressure (σ'_3) vs axial strain for 10 kPa consolidation pressure. Labels represent the void ratio e_c and the *RVD%* values for each specimen.

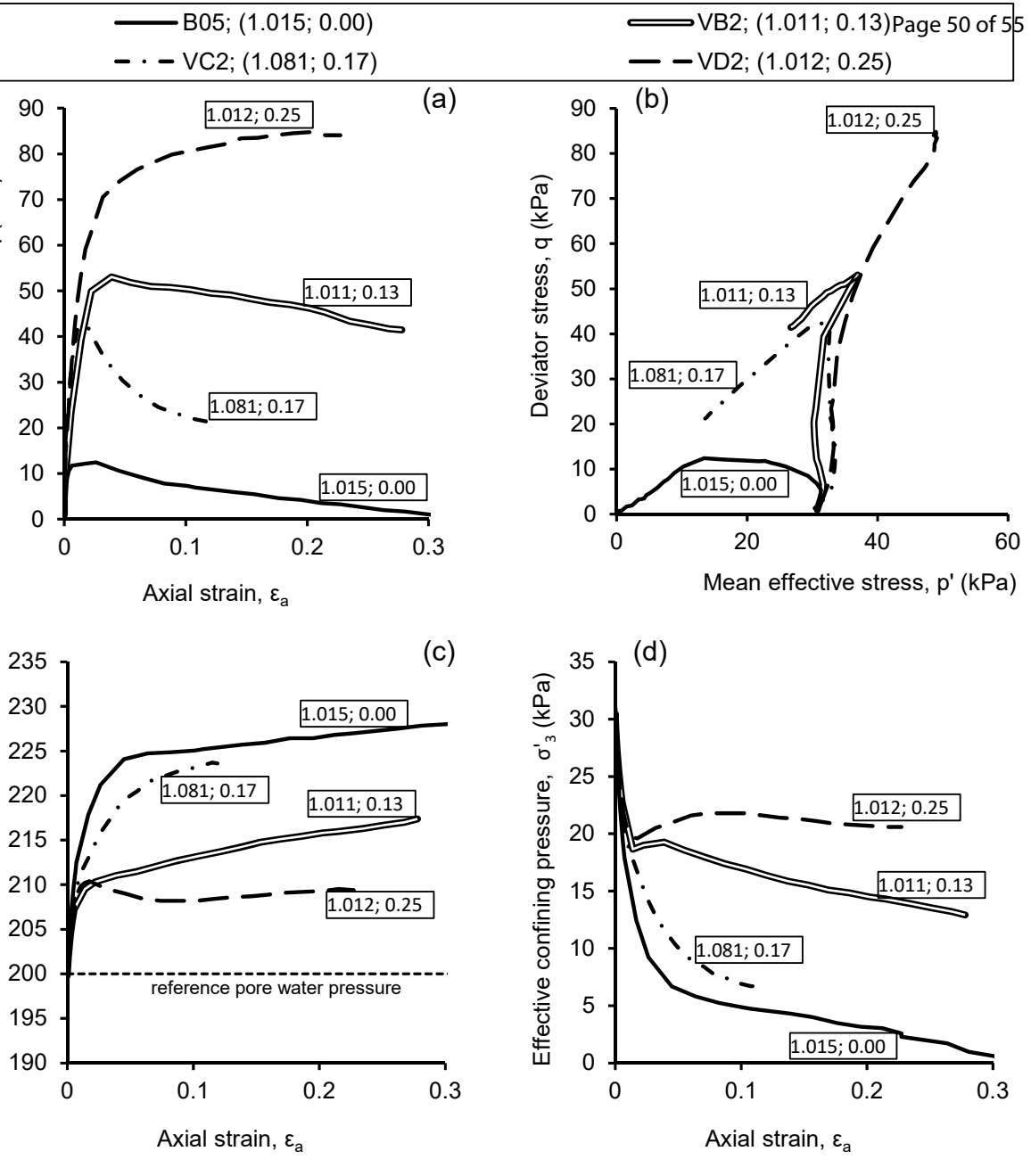

Figure 8. (a) Deviator stress (q_f) vs axial strain (ε_a); (b) Effective stress path in the Cambridge plane (q-p'); (c) Pore water pressure variation vs axial strain and (d) Effective confining pressure (σ'_3) vs axial strain for 30 kPa consolidation pressure. Labels represent the void ratio e_c and the *RVD%* values for each specimen.

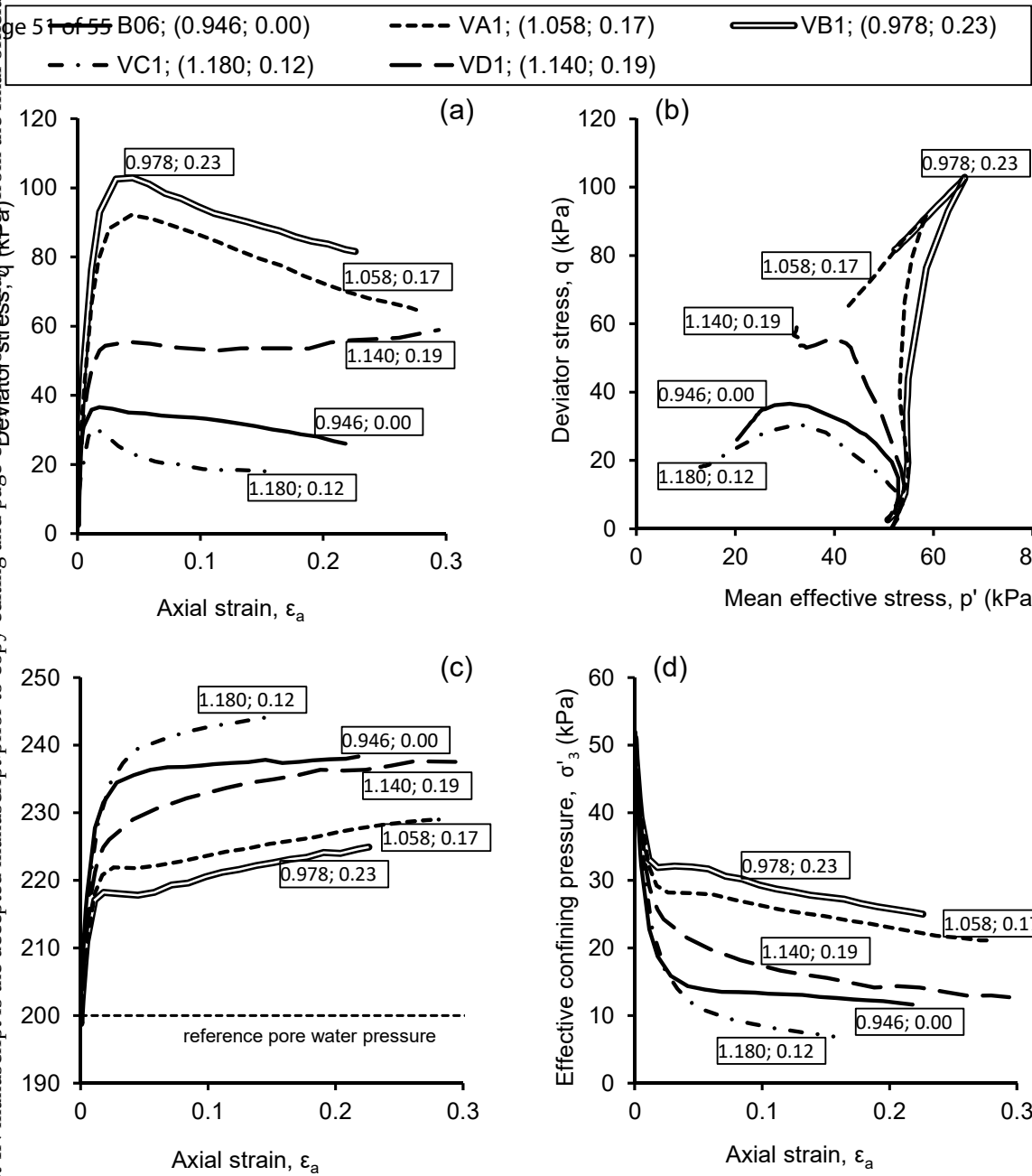

Figure 9. (a) Deviator stress (q_f) vs axial strain (ε_a); (b) Effective stress path in the Cambridge plane (*q-p'*); (c) Pore water pressure variation vs axial strain and (d) Effective confining pressure (σ'_3) vs axial strain for 50 kPa consolidation pressure. Labels represent the void ratio e_c and the *RVD%* values for each specimen.

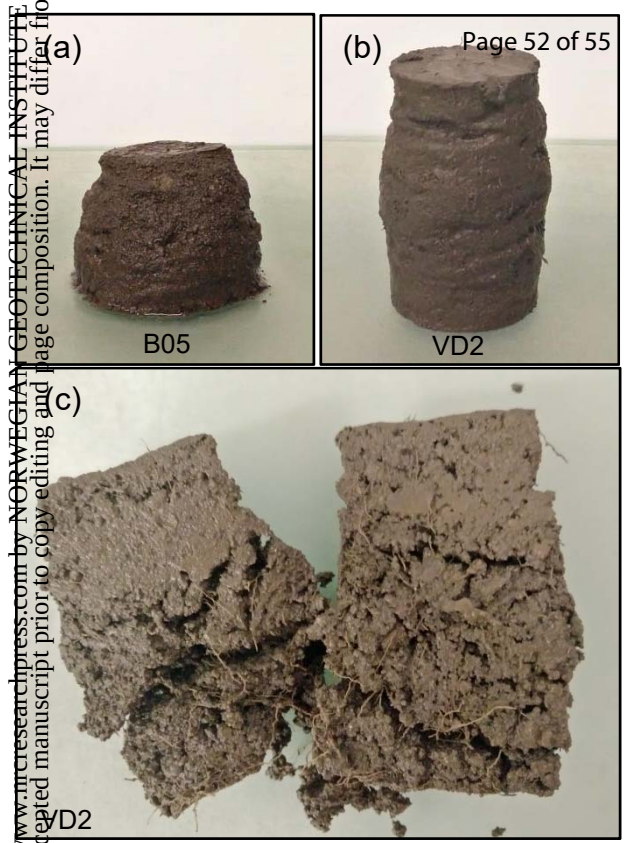

Figure10. Pictures of two specimens with the same void ratio (e_c=1.01): (a) bare soil; (b) rooted soil; (c) section of the rooted specimen at the end of the undrained shear stage.

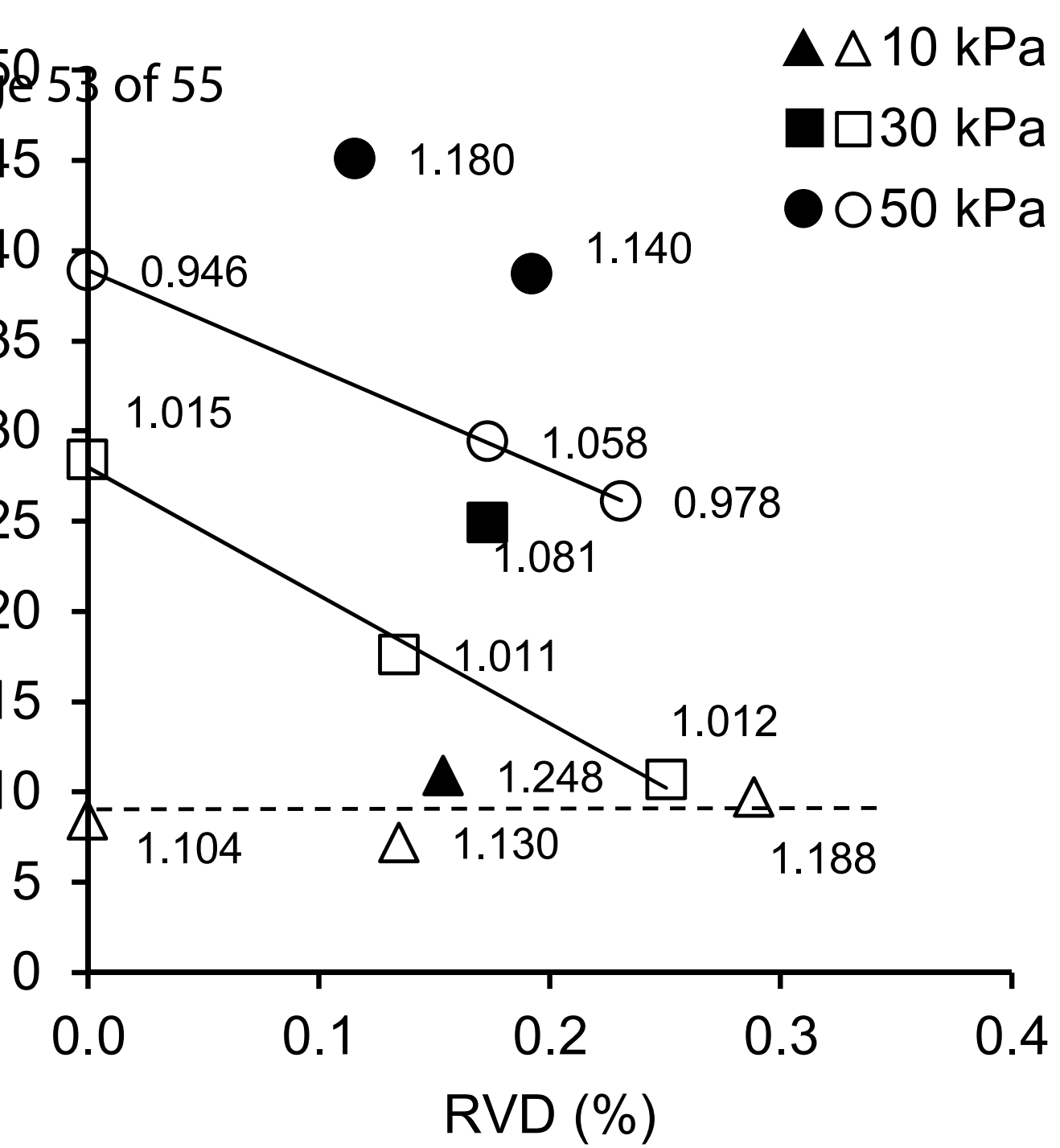

Figure11. Excess pore water pressures (Δu) vs *RVD* for 10, 30 and 50 kPa confining pressures. Labels represent the void ratio e_c, filled symbols correspond to the specimens having the highest void ratio among the others at the same consolidation pressure.

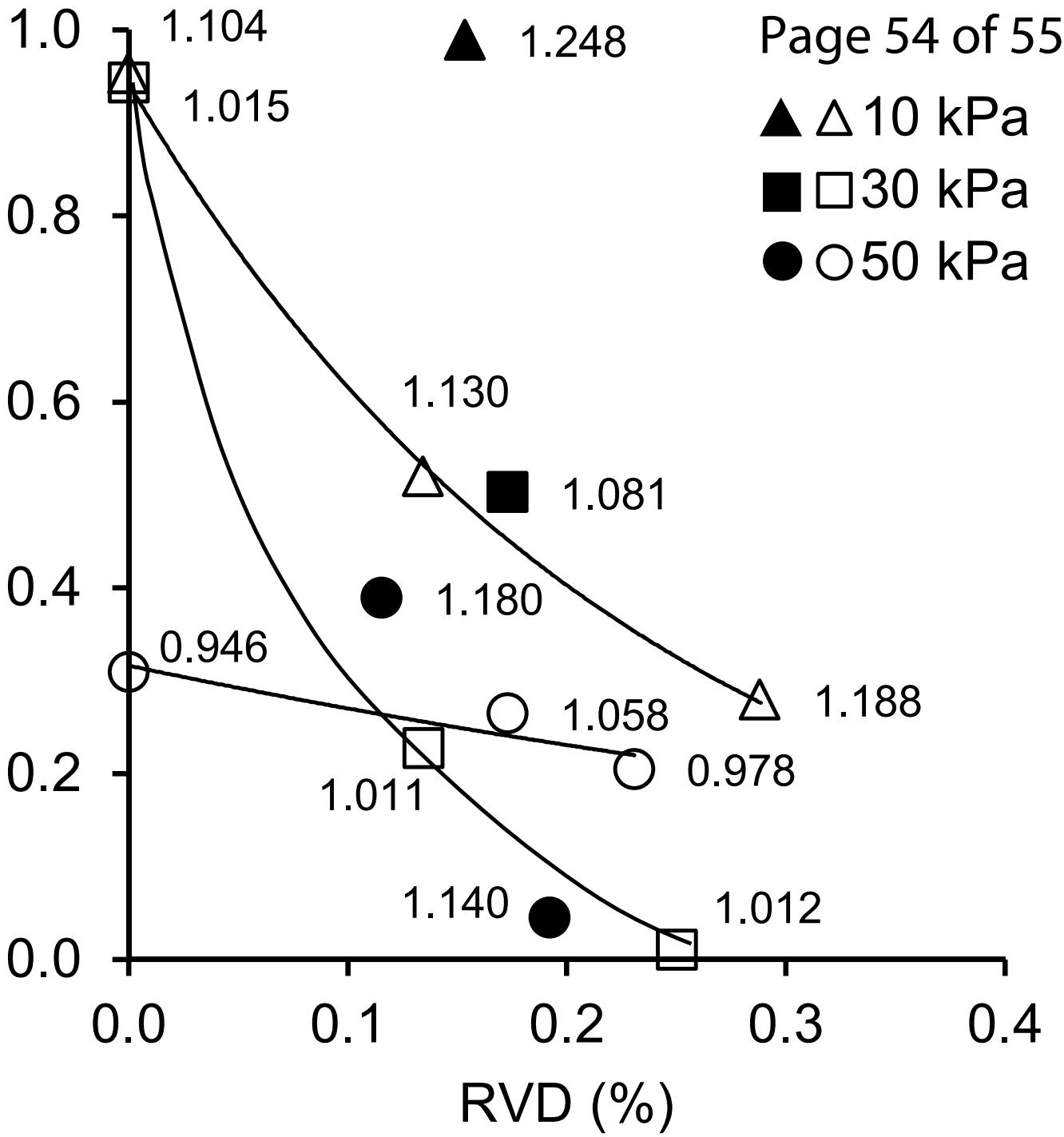

Figure12. Brittleness index (I_B) vs *RVD* for for 10, 30 and 50 kPa confining pressures. Labels represent the void ratio e_c, filled symbols correspond to the specimens having the highest void ratio among the others at the same consolidation pressure.

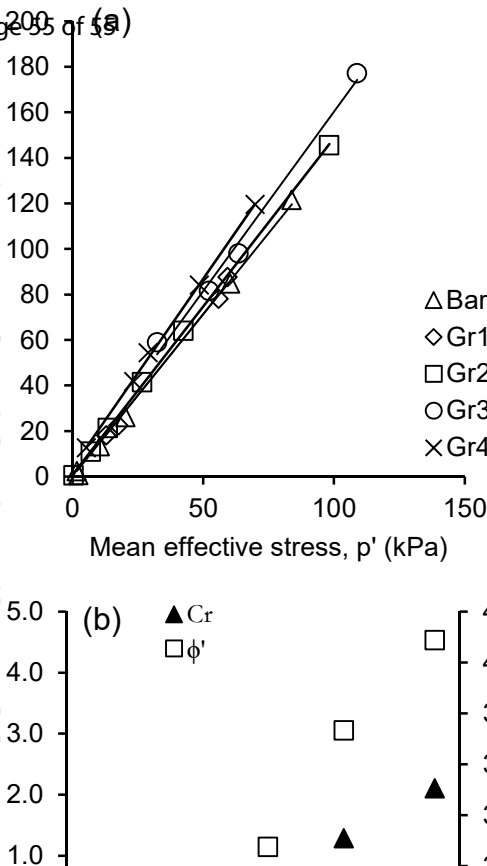

Figure13. (a) Failure envelopes in (*q-p'*) plane for vegetated specimens grouped in four classes of *RVD* and bare samples; (b) root cohesion (C_r) and integrated friction angle (ϕ') variations with RVD classes.